Corrosion behavior of alumina-forming austenitic stainless steels in Cl-based molten salt environment

Sumin Kim [a], Hyun Joon Eom [a], Won Seok Lee [b], Changheui Jang [a*]
[a]*Dept. of Nuclear and Quantum Engineering, KAIST, Daejeon, Rep. of Korea*
[b]*Dept. of Nuclear Engineering, Seoul National University, Seoul, Rep. of Korea*
[*]*Corresponding author: chjang@kaist.ac.kr*

***Keywords :** alumina forming austenitic stainless steels, molten salt, corrosion

1. Introduction

Currently, molten salt reactor (MSR), a Gen IV reactor system, is being widely researched for its inherent safety features and economic feasibility [1]. MSRs operate at atmospheric pressure, effectively mitigating the risk of severe accidents such as hydrogen explosions. However, identifying structural materials that meet the requirements of operating environment of MSRs like molten salt corrosion resistance, mechanical properties and irradiation resistance in high temperature remains a challenge. Furthermore, study of corrosion in molten chloride-based salt has been limited compared to that of fluoride-based salt.

In this study, a commercial alloy and Al-containing alloys developed by our research group were exposed to Cl-based molten salts at 750 °C for 500 hours. Al-containing alloys are advanced creep enhanced steel (ACES) [2] and newly developing alloy, advanced creep and radiation resistant stainless steels (ACRS). ACRS contains slightly higher contents of Al, Ni and Ti compared to existing alumina-forming austenitic (AFA) alloys and ACES. ACRS was thermo-mechanically processed in three different ways and subjected to the test.

After the corrosion test, weight change measurement, surface and cross-sectional analyses by electron microscope were conducted to evaluate the corrosion behavior of test materials.

2. Methods and Results

2.1 Alloy Design

The design of the newly developing alloy, ACRS, aimed to improve the corrosion, creep and radiation resistance as a structural material of MSRs. The Al content was selected to be near 5.5 wt.% for forming B2 phase which plays as an aluminum reservoir for forming alumina oxide layer providing corrosion resistance to molten salt environment [3] and provides desired mechanical properties to alloys at operating temperature of MSRs [4]. The Cr content was for air oxidation resistant property. In addition, the Ni content is for maintaining the fully austenitic matrix of alloy balancing with the Al and Cr contents. Meanwhile, the Ti content was selected to form gamma prime (γ') within the matrix to provide creep resistance [5]. The Nb and C contents were also selected to form Nb-rich carbide as a strengthening method of the alloy [6].

2.2 Material

One commercial alloy, Hastelloy N, along with two Al-containing alloys developed by our research group were used for molten salt corrosion test. For ACES (4.5% Al), a casting ingot of 1.2 kg was made by vacuum arc re-melting (VAR). After casting, ACES ingot was processed into plate through hot rolling and cold rolling. For ACRS (5.5% Al.), a casting ingot of 1.2 kg was made by vacuum pressure casting (VPC). In this study, as-cast ACRS, thermo-mechanically processed ACRS (ACRS-HR and ACRS-CR) were subjected to the molten salt corrosion test. The ingot of ACRS was heat-treated at 800 °C for 1 hour after processed into plate through hot rolling for ACRS-HR and cold rolling for ACRS-CR.

The thermo-mechanical processes of ACRS were determined to form fine B2 within the matrix using the result of thermodynamic simulation program, Thermo-Calc software (TCHEA-2 database). **Figure 1** shows that B2 exists along with γ' and Nb-rich carbide within austenitic matrix roughly from 720 ℃ to 980 ℃. **Figure 2** shows microstructure of as-cast ACRS, ACRS-HR and ACRS-CR. B2 phase was observed in all ACRS alloys and size of B2 is smaller in ACRS-HR and ACRS-CR compared to as-cast ACRS.

2.3 Molten Salt Corrosion Test

For the molten salt corrosion test, all materials were fabricated into coupon-type specimens with a diameter of 12 mm and a thickness of 1 mm by electrical discharge machining (EDM). A 1.5 mm of hole was drilled near the edge to hang the specimen on a Pt wire during testing. Prior to the corrosion test, the specimens were mechanically polished on both side using 1200 grit SiC paper and ultrasonically cleaned in ethanol.

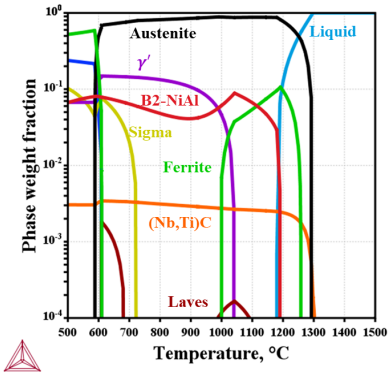

Fig. 1. Phase diagram of ACRS by thermodynamic simulation program (TCHEA-2 database)

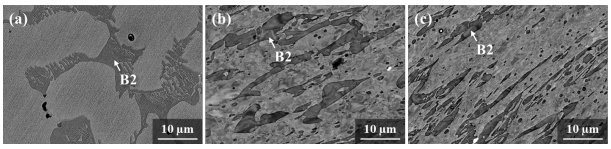

Fig. 2. SEM images of ACRS alloys: (a) as-cast ACRS, (b) ACRS-HR, (c) ACRS-CR

The anhydrous KCl (> 99 %) and NaCl (> 99 %) were supplied by Sigma Aldrich. The eutectic KCl-NaCl (50 mol.%-50 mol.%) was prepared within an Ar-filled glove box, with controlled ambient of oxygen and moisture content under 3 ppm each. To purify and stabilize the molten salt mixture, it was sustained at a temperature of 700 °C for 24 hours before the test. Two coupon specimens from each alloy were hung on a Pt wire within an alumina crucible, which has an inner diameter of 38 mm and a height of 103 mm. Each alumina crucible was charged with 51.5 g of the eutectic salt mixture to immerse the specimens. The static molten salt test was performed at 750 °C for 500 hours. After the test, specimens were carefully cleaned with distilled water to remove any residual salt.

Before and after the corrosion test, the weight of each specimen was measured using a microbalance (XP6, Mettler Toledo) with a resolution of 0.001 mg. For analyzing microstructural feature, scanning electron microscope (SEM) were carried out with Hitachi Su-8230 equipped with energy dispersion spectroscope (EDS).

2.4 Experimental results

Figure 3(a) shows the weight changes of test materials after molten KCl-NaCl corrosion test at 750 °C for 500 hours. Every material tested shows weight loss but at different degree. The weight loss of the specimens in decreasing order is ACRS-HR > ACRS-CR > Hastelloy N > ACES > as-cast ACRS. However, it is not easy to evaluate the corrosion resistance of test materials accurately only with the weight changes result. Thus, further surface and cross-sectional analyses were carried out.

For surface analysis, except Hastelloy N, all specimens show alumina layer formed on the surface. However, the alumina layer was spalled. For cross-sectional analysis, uniform Cr-depleted and B2-denuded depths of test materials are shown in **Fig. 3**(b), (c), respectively. Both Hastelloy N and ACES show less than 2 μm of Cr-depleted depth after exposure. Among ACRS alloys, only ACRS-HR shows 3.5 μm of Cr-depleted depth after exposure which is biggest among all tested alloys. Nevertheless, all ACRS alloys show B2-denude zone which Hastelloy N and ACES show none.

Although the spallation of alumina layer has been observed in all ACRS alloys, it can be said that this spallation has occurred after finishing the corrosion test considering that no Cr-depleted zone has been observed in as-cast ACRS and ACRS-CR. In other words, alumina layer was spalled after corrosion test, during the cooling process due to the residual stress generated from thermal expansion difference between substrate metal and oxide layer [7].

Meanwhile, as mentioned above, ACRS-HR still showed Cr-depleted zone, indicating that it had a different corrosion mechanism from the other ACRS alloys. To investigate this corrosion mechanism of ACRS-HR, further detailed microstructure analysis of ACRS alloys are being conducted with transmission electron microscopy (TEM). The TEM analyses were carried out with the FEI-Talos F200X equipped with a Bruker Quantax EDS at the voltage of 200 kV. ACRS-HR was fabricated into thin foil specimens with a diameter of 3 mm and mechanically polished until a thickness of about 100 μm. Then, the specimens were subjected to twin-jet electropolishing at -30 °C with a current of about 0.1 A in a solution of 10 % perchloric acid + 90 % methanol. **Figure 4** shows γ' with a diameter of about 200 nm within the ACRS-HR austenitic matrix. Since, the γ' ($Ni_3(Al, Ti)$) is formed competitively with B2 (NiAl) due to its similar chemical compositions (**Fig. 1**), controlling the size of γ' and more detailed microstructure analysis are being conducted to check whether secondary phases have an effect on formation of stable alumina. Furthermore, to evaluate the quantitative characteristics of alumina formation of ACRS alloys, for instance, growth rate of alumina and saturation time of alumina, electrochemical impedance spectroscopy (EIS) is planned in Cl-based molten salt environment.

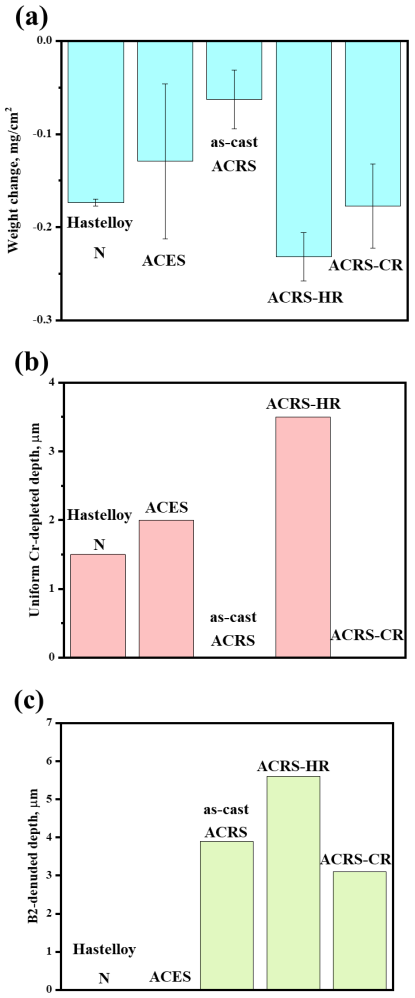

Fig. 3. (a) Weight change, (b) uniform Cr-depleted depth, and (c) B2-denuded depth of tested alloys after exposure to molten KCl-NaCl salts at 750 °C for 500 hours

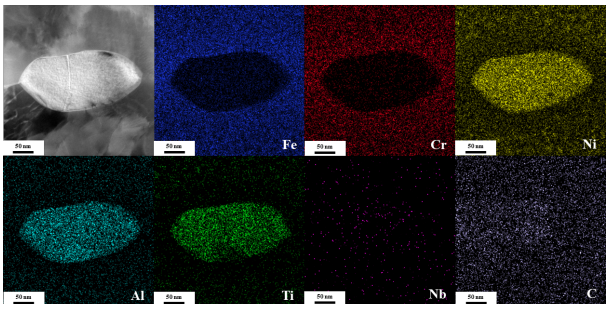

Fig. 4. STEM/EDS mapping images of **γ'** formed in austenitic matrix of ACRS-HR alloy

3. Conclusions

Molten salt corrosion behavior of commercial alloy (Hastelloy N) and Al-containing developed alloys (ACES and ACRS) were investigated after exposure to KCl-NaCl at 750 °C for 500 hours. All tested alloys showed weight loss, but at different degree. Alumina layer was formed in all Al-containing alloys but seemed to be spalled during the cooling process. In addition, both Hastelloy N and ACES showed less than 2 μm of Cr-depleted depth. Among ACRS alloys, only ACRS-HR showed Cr-depletion depth. To investigate different corrosion mechanisms of ACRS alloys which were varied in thermos-mechanical processes, further microstructure analyses for ACRS are being conducted.

REFERENCES

[1] Guo S, Zhang J, Wu W, Zhou W, Corrosion in the molten fluoride and chloride salts and materials development for nuclear applications, Progress in Materials Science, Vol.97, pp.448-487, 2018.
[2] Subramanian GO, Kim C, Heo W, Jang C, Corrosion behaviour of alumina-forming heat resistant alloy with Ti in high temperature steam, Corrosion Science, Vol.195, 110000, 2022.
[3] Brady MP, Yamamoto Y, Santella ML, Walker LR, Composition, microstructure, and water vapor effects on internal/external oxidation of alumina-forming austenitic stainless steels, Oxidation of metals, Vol.72, pp.311-333, 2009.
[4] Zhou D, Zhao W, Mao H, Hu Y, Xu X, Sun X, et al., Precipitate characteristics and their effects on the high-temperature creep resistance of alumina-forming austenitic stainless steels, Materials Science and Engineering: A, Vol.622, pp.91-100, 2015.
[5] Pike L, Development of a fabricable gamma-prime (γ′) strengthened superalloy. Superalloys 2008, pp.191-200, 2008.
[6] Zhao W, Zhou D, Jiang S, Wang H, Wu Y, Liu X, et al., Ultrahigh stability and strong precipitation strengthening of nanosized NbC in alumina-forming austenitic stainless steels subjecting to long-term high-temperature exposure, Materials Science and Engineering: A, Vol.738, pp.295-307, 2018.
[7] Tolpygo V, Clarke D, Spalling failure of α-alumina films grown by oxidation: I. Dependence on cooling rate and metal thickness, Materials Science and Engineering: A, Vol.278, pp.142-150, 2000.